Aalborg Universitet

Design-Oriented Analysis of Resonance Damping and Harmonic Compensation for LCL-Filtered Voltage Source Converters

Wang, Xiongfei; Blaabjerg, Frede; Loh, Poh Chiang

Design-Oriented Analysis of Resonance Damping and Harmonic Compensation for *LCL*-Filtered Voltage Source Converters

Xiongfei Wang, Frede Blaabjerg, and Poh Chiang Loh
Department of Energy Technology, Aalborg University, Aalborg, Denmark
xwa@et.aau.dk, fbl@et.aau.dk, pcl@et.aau.dk

Abstract— **This paper addresses the interaction between harmonic resonant controllers and active damping of *LCL* resonance in voltage source converters. A virtual series R-C damper in parallel with the filter capacitor is proposed with the capacitor current feedback loop. The phase lag resulting from the digital computation and modulation delays is thus compensated by the virtual capacitor. The frequency region that allows using resonant controllers is then identified with the virtual damper. It reveals that the upper frequency limit of harmonic resonant controllers can be increased above the gain crossover frequency defined by the proportional gain of current controller. This is of particular interest for high-performance active harmonic filtering applications and low-pulse-ratio converters. Case studies in experiments validate the theoretical analysis.**

Keywords— *Harmonic compensation, resonant controller, active damping, LCL resonance*

I. INTRODUCTION

LCL filters have widely been found in grid-connected voltage source converters, owing to their better switching ripple attenuation and smaller volumes compared to *L* filters [1]. But on the other hand, the *LCL* resonance characteristic challenges the current control of converters and worsens the sensitivity to grid voltage harmonics [2]. These issues may be exacerbated in paralleled converters with *LCL* filters such as in renewable power plants and microgrids, in which multiple resonance frequencies may be introduced challenging the system stability [3], [4]. Furthermore, with the increased penetration of nonlinear load, the harmonic distortion in the power grids is getting worse. The control of current harmonics is important for grid-connected converters to meet the grid codes and to furnish the active harmonic filtering functions [5].

The design of resonant current controllers for voltage source converters with *L* filters has been well developed, where the harmonics up to the Nyquist frequency can be controlled [6]-[8]. However, for *LCL*-filtered converters, the use of resonant controllers is challenged by the *LCL* resonance, and particularly for the harmonics close to the resonance frequency of the filter. Traditionally, the resonant controllers are merely employed below the gain crossover frequency of the current control loop which is

defined by the proportional gain [4], [9], [10]. Thus, the stability of resonant controllers can be decoupled from the effect of *LCL* resonance, whereas the frequency range of harmonic compensation is limited compared to the converters with *L* filters. This drawback may be more obvious for low-pulse-ratio converters in which the ratio of the switching frequency to the fundamental frequency is low [11], [12]. The variation of grid impedance is another challenge in this case, which may shift the gain crossover frequency in a wide range and may reduce the Phase Margin (PM) of the resonant controllers near the gain crossover frequency resulting in unstable harmonic compensation [10]. It is, therefore, of particular interest to broaden the frequency region for resonant controllers by means of *LCL* resonance damping techniques.

Extensive research has gone into the damping of *LCL* filter resonance for voltage source converters, which can be attained by either passive dampers or active damping control concept [13]-[15]. Among these approaches, the capacitor-current-based active damping control is found easy-to-use and effective [2], [15]-[20]. In this method, the proportional gain of the capacitor current feedback loop is basically equivalent to a virtual resistor in parallel with the filter capacitor [17]. But considering the effect of the digital computation and Pulse Width Modulation (PWM) delays, the virtual resistor turns into a virtual impedance. The imaginary part of this virtual impedance changes the actual *LCL* resonance frequency, while the real part may be negative depending on the ratio of the *LCL* resonance frequency to the control frequency [18]. Such a negative virtual resistance brings the open-loop Right Half-Plane (RHP) poles into the current control loop resulting in a non-minimum phase behavior [19].

Several solutions have recently been reported to avoid the non-minimum phase system induced by the capacitor-current-based active damping. A direct way is to reduce the computation delay by shifting the sampling instant of the capacitor current [19]. It is easy to implement but is susceptible to the aliasing of capacitor current. Another attractive way is to predict the capacitor current by means of either the observer [20], or the discrete-time derivative controller [21]. A good robustness of resonance damping against the grid impedance variation is obtained in these works, yet few of them addresses the interaction of the active damping with resonant controllers and, particularly

when the current harmonics close to the *LCL* resonance frequency need to be controlled.

This paper presents a design-oriented analysis for the interaction of the capacitor-current-based active damping and the harmonic resonant controllers. A virtual series R-C damper in parallel with the filter capacitor is proposed by means of a first-order high-pass filter in the capacitor current feedback loop. Thus, the effect of computation and PWM delays in the active damping can be mitigated by the virtual capacitor. Then, based on the virtual R-C damper, the frequency region that allows using harmonic resonant controllers is investigated. The effect of active damping control parameters on the stability of resonant controllers is analyzed. It shows that with a robust design of active damping, the resonant controller can be applied for the harmonics above the gain crossover frequency defined by the proportional gain of current control loop. The design constraint of the virtual series R-C damper is thus formulated. Case studies in experiments validate the theoretical analysis.

II. REVIEW OF CAPACITOR-CURRENT-BASED ACTIVE DAMPING AND HARMONIC RESONANT CONTROLLERS

A. System Description

Fig. 1 illustrates a three-phase grid-connected voltage source converter with the *LCL* filter. The DC-link voltage is assumed to be constant, and the bandwidth of the grid synchronization loop is designed to be lower than the grid fundamental frequency in order not to induce instabilities [22]. The grid current (i_2) is controlled synchronous with the Point of Common Coupling (PCC) voltage. The main parameters of the converter are listed in Table I, which are used in this study.

Fig. 2 depicts the per-phase diagram of the grid current control, since the three-phase systems without the neutral wire can be transformed into two decoupled single-phase systems in the stationary $\alpha\beta$-frame [23]. $G_c(s)$ denotes the proportional plus multi-resonant current controllers. $G_d(s)$ represents the effect of the digital computation and PWM delays in the continuous form, which are given by

$$G_c(s) = K_p + \frac{K_{i1}s}{s^2 + \omega_1^2} + \sum_{h=5,7,\dots n} K_{ih} \frac{s\cos(\theta_h) - h\omega_1\sin(\theta_h)}{s^2 + h^2\omega_1^2}$$
(1)

$$G_d(s) = e^{-1.5T_s s}$$
(2)

where ω_1 is the fundamental frequency of grid, T_s is the sampling period, and θ_h is the phase leading angle.

B. Capacitor-Current-Based Active Damping

The capacitor-current-based active damping is attained by a proportional feedback of the filter capacitor current, as depicted in Fig. 2. Thus, a double-loop current control structure is formed with the grid current feedback loop. The instability of the inner active damping loop results in a non-minimum phase behavior of the outer grid current control loop, which consequently imposes the constraint on the design of the current controller [16].

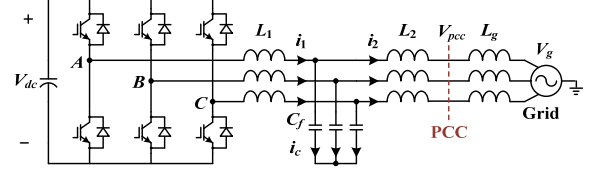Fig. 3 illustrates the physical insight of the inner active

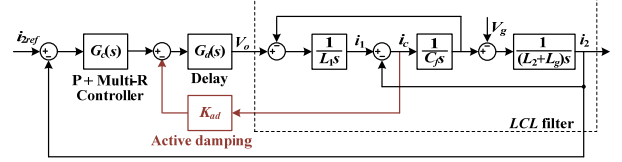Fig. 1. Three-phase grid-connected voltage source converter with the *LCL* filter.

Fig. 2. Per-phase diagram of the grid current control with the capacitor-current-based active damping.
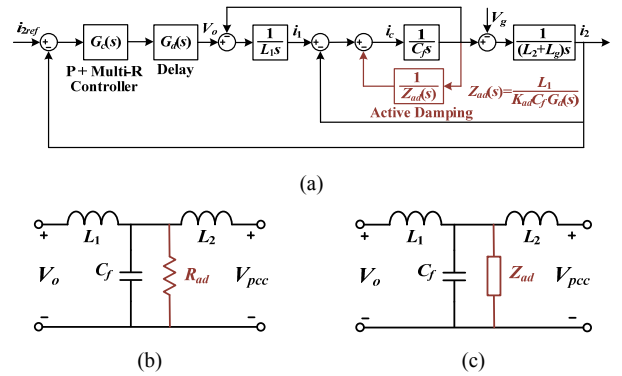

Fig. 3. Equivalent transformation of the capacitor-current-based active damping loop. (a) Block diagram representation. (b) Equivalent circuit of the *LCL* filter without the delay effect. (c) Equivalent circuit of the *LCL* filter with the delay effect.

TABLE I
MAIN PARAMETERS OF GRID-CONNECTED CONVERTER

Symbol	Meaning	Value
V_g	Grid voltage	400 V
f_1	Grid frequency	50 Hz
f_{sw}	Switching frequency	10 kHz
f_s	Sampling frequency	10 kHz
T_s	Sampling period	100 μs
V_{dc}	DC-link voltage	800 V
L_1	Filter inductor 1	3.6 mH
L_2	Filter inductor 2	1 mH
C_f	Filter capacitor	4.7 μF

damping loop by means of block diagram transformation. It is seen that the virtual resistor in parallel with the filter capacitor is basically synthesized by the proportional gain (K_{ad}), which is shown in Fig. 3 (b). However, considering the effect of computation and PWM delays, the virtual resistor turns into the virtual impedance, as shown in Fig. 3(c), which is given by [19]

$$Z_{ad}(j\omega) = \frac{L_1}{K_{ad}C_f}[\cos(1.5\omega T_s) + j\sin(1.5\omega T_s)]$$
(3)

Consequently, the actual *LCL* resonance frequency is changed by the imaginary part of virtual impedance. The real part of virtual impedance becomes negative when the

LCL resonance frequency is between the one-sixth of the control frequency ($\omega_s/6$) and the Nyquist frequency ($\omega_s/2$). The negative resistance brings the open-loop RHP poles into the outer grid current control loop.

It is worth noting that the frequency $\omega_s/6$ has been identified as the critical frequency in grid current control loop and the active damping is only needed for the *LCL* resonance frequency higher than $\omega_s/6$ [17]. However, the wide variation of grid impedance in weak grids shifts the *LCL* resonance frequency across $\omega_s/6$, which may result in unstable grid current control loop, when the resonance frequency is close to $\omega_s/6$.

C. Harmonic Resonant Controllers

The implementation of resonant current controllers has been well documented in [6]-[8]. The current harmonics up to the Nyquist frequency can be compensated with a proper discretization method and phase compensation.

Fig. 4 (a) depicts the basic structure of the resonant current controller based on two integrators. It consists of the forward and backward Euler integrators. The transfer function can be derived as

$$G_{Rh}(z) = K_{ih}T_s \frac{z^{-1}\left[\cos(\theta_h) - h\omega_1 T_s \sin(\theta_h)\right] - z^{-2}\cos(\theta_h)}{1 - 2z^{-1}(1 - h^2\omega_1^2 T_s^2/2) + z^{-2}} \tag{4}$$

This form of discretization is computationally efficient but with low accuracy resulting from the displacement of resonant poles and zeros. The term $(1 - h^2\omega_1^2 T_s^2/2)$ in the denominator of (4) is a second-order Taylor series of the trigonometric term $\cos(h\omega_1 T_s)$ required for the accurate placement of resonant poles [7]. The discrepancy leads to the frequency errors of resonant peaks, which are further exacerbated with the increase of T_s and $h\omega_1$ [8]. Further, compared to the resonant controller with accurate phase compensation, which is given by

$$G_{Rh}(z) = K_{ih}T_s \frac{\cos(\theta_h) - z^{-1}\cos(\theta_h - h\omega_1 T_s)}{1 - 2z^{-1}\cos(h\omega_1 T_s) + z^{-2}} \tag{5}$$

a correction of zeros is needed for the resonant controller with two integrators to obtain good performance.

Fig. 4 (b) shows the diagram of the resonant controller with the improved accuracy [8], which is adopted in this work for harmonic compensation. The sixth-order Taylor series of $\cos(h\omega_1 T_s)$ is used for the correction of resonant poles, and the phase lead input is modified to reduce the inaccuracies of zeros.

The improved resonant controller works well in the *L*-filtered converters, as the phase lead θ_h is readily derived. However, for the *LCL*-filtered converters, the calculation of phase lead is complicated by the phase change around the *LCL* resonance frequency. Also, the non-minimum phase behavior induced by the inner active damping loop limits the frequency range for stable resonant controllers. Hence, it is needed to identify the upper frequency limit of using harmonic resonant controllers in the *LCL*-filtered converters.
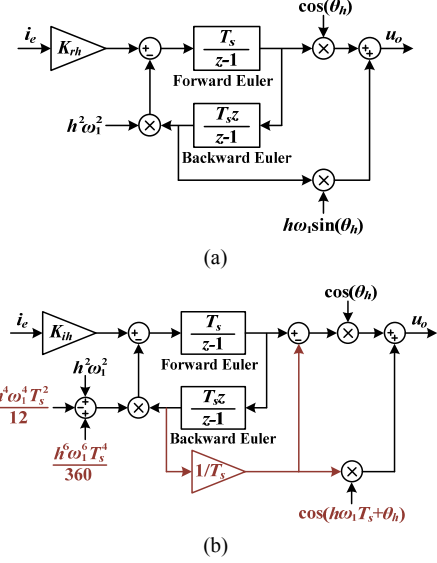

(a)

(b)

Fig. 4. Block diagrams of the resonant controller with two integrators. (a) Basic structure. (b) Improved structure.

III. PROPOSED VIRTUAL SERIES R-C DAMPER

A. Basic Principle

Fig. 5 shows the block diagram of the proposed active damping control scheme. Unlike the proportional gain in Fig. 2, the first-order high-pass filter is introduced in the capacitor current feedback loop.

First, in order to see the physical property of the high-pass filter, the effect of computation and PWM delays is neglected. Fig. 6 shows the equivalent circuit of the *LCL* filter with the high-pass filter. It is seen that the virtual series R-C damper in parallel with the filter capacitor is synthesized, which can be given by

$$R_{rc} = \frac{L_1}{K_{rc}C_f}, \quad C_{rc} = \frac{K_{rc}C_f}{L_1\omega_{rc}}, \quad \omega_{rc} = \frac{1}{R_{rc}C_{rc}} \tag{6}$$

where K_{rc} and ω_{rc} are the gain and cut-off frequency of the high-pass filter, respectively.

Then, considering the delay effect, the virtual damper is changed as the following virtual impedance

$$Z_{rc}(j\omega) = \frac{L_1}{K_{rc}C_f}(1 - j\frac{\omega_{rc}}{\omega})\left[\cos(1.5\omega T_s) + j\sin(1.5\omega T_s)\right] \tag{7}$$

Thus, the frequency at which the real part of the virtual impedance becomes negative (ω_{nr}) can be derived, which is plotted in Fig. 7 as a function of the cut-off frequency of the high-pass filter. It can be seen that at the zero cut-off frequency, $\omega_{nr} = \omega_s/6$. As the increase of the filter cut-off frequency, ω_{nr} is increased.

B. Comparative Analysis in Frequency-Domain

To illustrate the effect of the proposed active damping approach, a comparative analysis with the conventional capacitor-current-based active damping for the different grid inductances is presented in the following. Table II summarizes the main controller parameters.

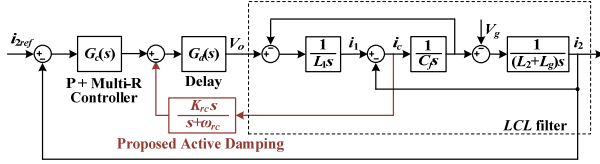Fig. 8 shows the frequency response of the open-loop

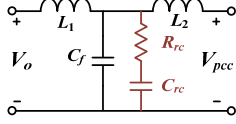Fig. 5. Block diagram of the proposed active damping control scheme.

Fig. 6. Equivalent circuit of the *LCL* filter with the high-pass filter.
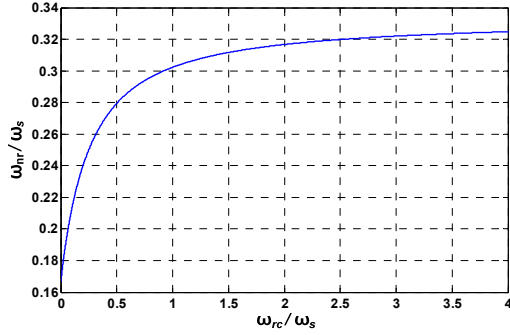

Fig. 7. Relationship between the frequency where the virtual resistance becomes negative and the cut-off frequency of high-pass filter.

TABLE II
MAIN CONTROLLER PARAMETERS

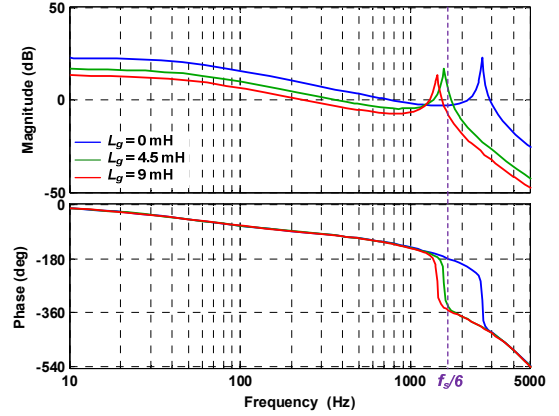| Symbol	Meaning	Value
K_p	Proportional gain	20
K_{i1}	Fundamental frequency resonant controller gain	1000
K_{ih}	Harmonic resonant controllers gains	1000
K_{rc}	High-pass filter gain	15
ω_{rc}	Cut-off frequency of high-pass filter	$0.2\omega_s$ rad/s

Fig. 8. Frequency response of the open-loop gain of the grid current control with the proportional current controller only.
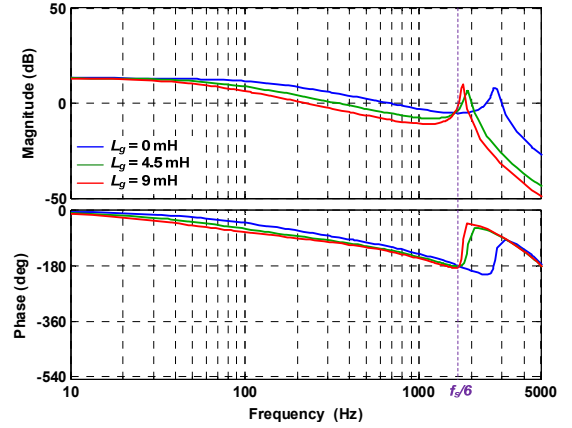

Fig. 9. Frequency response of the open-loop gain of the grid current control with the conventional capacitor-current-based active damping.
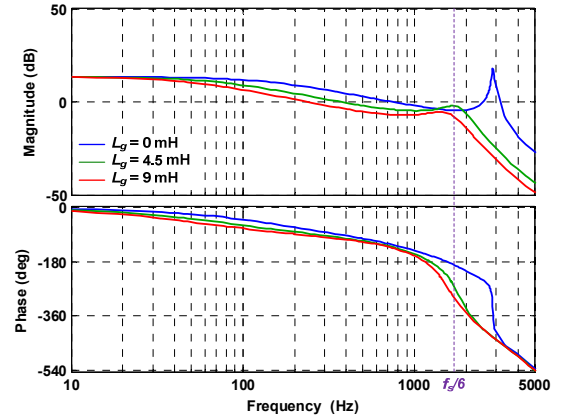

Fig. 10. Frequency response of the open-loop gain of the grid current control with the proposed virtual series R-C damper.

gain of the grid current control loop with the proportional current controller only. The proportional gain is designed based on the *LCL* filter inductors (L_1+L_2) with the PM of 45°[16]. It can be seen that the *LCL* resonance frequency is reduced as the increase of grid inductance, and the current control loop turns unstable when the resonance frequency is below $\omega_s/6$.

Fig. 9 shows the frequency response of the open-loop gain of grid current control loop with the conventional capacitor-current-based active damping control. The non-minimum phase behavior induced by the negative virtual resistance is observed. Instead of the resonance damping, the resonant peaks are shifted by the virtual impedance. Based on the Nyquist stability criterion, it is found that the system are stable for the cases of L_g=0 mH and L_g=9 mH, and are marginally stable for the case of L_g=4.5 mH. This is because the resonance frequency in this case is closer to the frequency for negative virtual resistance ω_{nr}.

Fig. 10 shows the frequency response of the open-loop gain of grid current control loop with the proposed virtual series R-C damper. The non-minimum phase behavior is mitigated by the virtual capacitor. The resonant peaks are

well dampened for the cases of L_g=4.5 mH and L_g=9 mH, while the resonant peak is shifted in the case of L_g=0 mH. This is because the frequency ω_{nr} is shifted closer to the resonance frequency in the case of L_g=0 mH.

IV. DESIGN-ORIENTED ANALYSIS

A. Design of Virtual Series R-C Damper

In order to achieve a robust design of the virtual series R-C damper against the grid impedance variation, a root locus analysis in the *z*-domain is presented as follows:
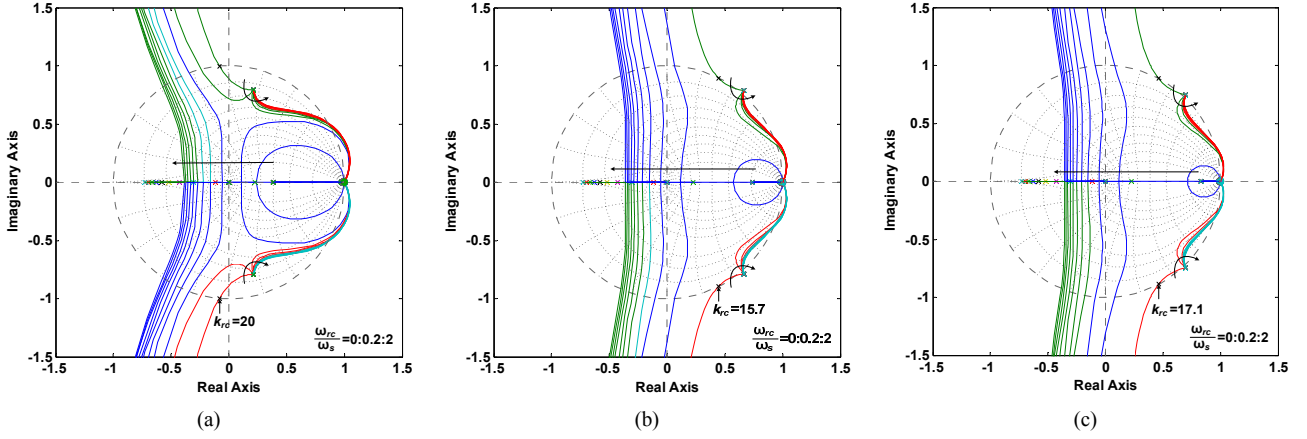
Fig. 11. Root loci of the outer grid current control loop with the different grid inductance (L_g) in the discrete-time z-domain. (a) L_g=0 mH, f_{res}=2.6 kHz. (b) L_g=4.5 mH, f_{res}=1.57 kHz. (c) L_g=9 mH, f_{res}=1.42 kHz.

The Zero-Order-Hold (ZOH) transform is used for the transfer function from the inverter output voltage to filter capacitor current, and the impulse invariant transform is applied for the transfer function of filter capacitor current to grid current [16], which are given by

$$G_{vc}(s) = \frac{i_c}{V_o}\bigg| = \frac{1}{L_1}\frac{s}{\left(s^2+\omega_{res}^2\right)}, \quad G_{cg}(s)=\frac{i_g}{i_c}=\frac{1}{L_{to}C_f s^2}$$
(8)

$$G_{vc}(z) = \frac{\sin(\omega_{res}T_s)}{\omega_{res}L_1}\frac{(z-1)}{\left[z^2-2z\cos(\omega_{res}T_s)+1\right]}$$
(9)

$$G_{cg}(z) = \frac{T_s z}{\left(L_2+L_g\right)C_f\left(z-1\right)^2}$$
(10)

where ω_{res} is the LCL resonance frequency. The high-pass filter is discretized by the Tustin transform.

Fig. 11 depicts the effect of the high-pass filter gain K_{rc} on the closed-loop poles trajectory of the grid current control loop, and the different cut-off frequencies of the high-pass filter are swept with different grid inductances.

Fig. 11 (a) shows that the poles track well inside the unit circle for L_g=0 mH, owing to the inherent damping effect of the computation and PWM delays. In contrast, in Figs. 11 (b) and (c), the poles are initially outside the unit circle and track back inside with the increase of K_{rc}. This is because the resonance frequencies in these cases are lower than ω_s/6. The stable region of K_{rc} is reduced as the resonance frequency becomes closer to the frequency for the virtual resistance becoming negative (ω_{nr}). Also, Figs. 11 (b) and (c) show that the cases with resonance frequency close to ω_{nr} has less damping.

In all three cases, the increase of the cut-off frequency ω_{rc} forces the poles to track inside the unit circle, and the stable region of K_{rc} is broadened. However, the change of root loci becomes small for high ω_{rc}. This agrees with the analysis in Fig. 7 where the ω_{nr} has few change for high ω_{rc}. Hence, to design the virtual series R-C damper, the frequency ω_{rc} can first be determined from Fig. 7 in order

that the frequency ω_{nr} is well separated from the range of LCL resonance frequency. Then the root locus analysis in Fig. 11 can be used to find the high-pass filter gain.

B. Frequency Region of Harmonic Control

From Fig. 8, it can be observed that the gain crossover frequency is significantly reduced as the increase of grid inductance. The frequency region of the harmonic control is limited if resonant controllers are only applied below the gain crossover frequency. Consequently, the resonant controllers with proper phase compensation are needed to broaden the frequency region of harmonic control.
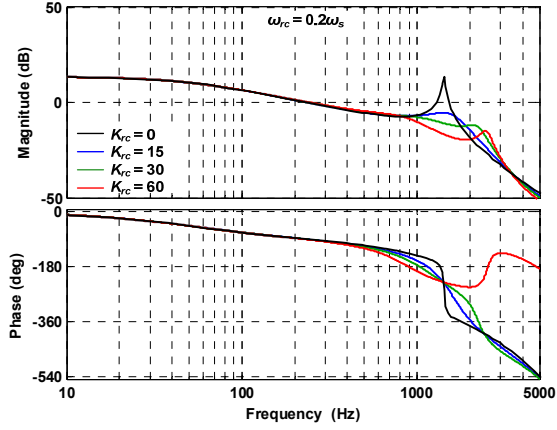
Basically, the LCL resonance frequency imposes the upper frequency limit of resonant controllers, due to the sharp phase transition at the LCL resonance frequency. The phase leading angle of the resonant controllers below the LCL resonance frequency can be approximated as

$$\theta_h = \frac{\pi}{2}+1.5h\omega_1 T_s$$
(11)

However, from Fig. 10, it is seen that the virtual series R-C damper brings in phase change for the frequencies near the LCL resonance. Using (11) may cause the inaccurate phase compensation of resonant controllers.

Fig. 12 depicts the effect of the high-pass filter on the phase change around the LCL resonance frequency in the case of L_g=9 mH. Fig. 12 (a) depicts the effect of K_{rc} for the case of ω_{rc}=0.2ω_s. It is seen that the phase lag caused by the high-pass filter is increased with K_{rc}. Fig. 12 (b) depicts the case of ω_{rc}=3ω_s. Compared to Fig. 12 (a), it is clear that the increase of ω_{rc} requires an increase of K_{rc} in order to obtain the same level of damping. The phase lag is further increased for the same level of damping.

Fig. 13 depicts such phase lag effect on the stability of harmonic resonant controller. Two high-pass filters with the same level of damping but the different ω_{rc} and K_{rc} are compared. The phase leading angles for the resonant controllers are calculated by (11). It can be seen that the phase lag resulting from the increase of ω_{rc} reduces the PM of the high-order harmonic resonant controllers (23rd) and even result in instability (25th). Hence, apart from the presence of the negative virtual resistance, the stability of
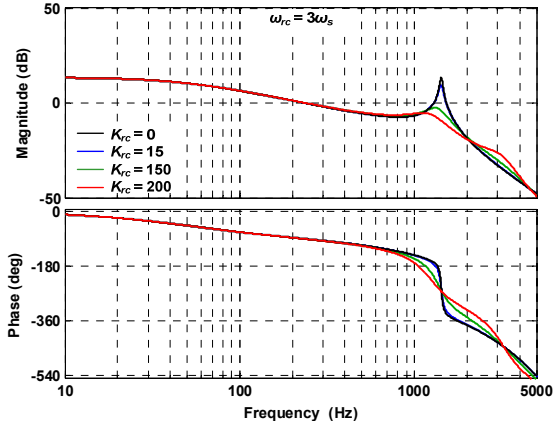
Fig. 12. Effect of high-pass filters on the phase change close to the *LCL* resonance frequency. (a) Low cut-off frequency ($\omega_{rc}=0.2\omega_s$). (b) High cut-off frequency ($\omega_{rc}=3\omega_s$).

Fig. 13. Comparison between the effect of phase lag resulting from the different high-pass filter design. (a) Full view. (b) Zoomed out for the 23rd and 25th harmonic resonant controllers.

resonant controllers for the harmonics near the resonance frequency imposes the upper limit on the value of the cut-off frequency of high-pass filter.
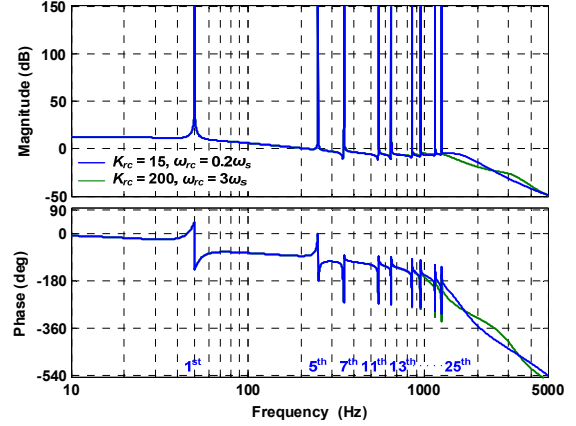
V. EXPERIMENTAL RESULTS

To validate the theoretical analysis, the experimental case studies are carried out based on the parameters listed in Table I and II. The California Instruments MX-series AC power source is used for grid emulation. The Danfoss frequency converter powered by the constant DC voltage source is controlled as the grid-connected voltage source converter. The control system is implemented in DS1006 dSPACE system, where the DS5101 is used for the PWM generation in synchronous with the Analog/Digital (A/D) sampling circuit.
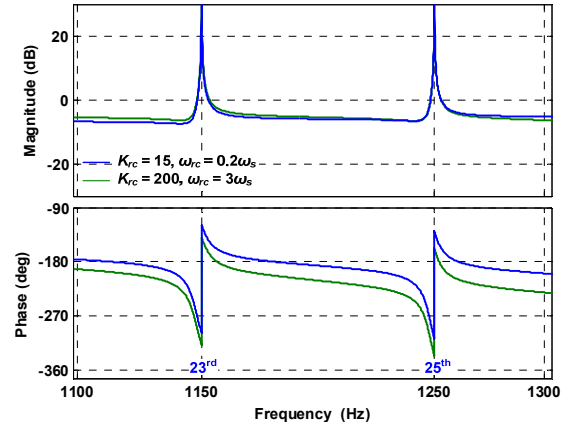
A. Active Damping of LCL resonance

Fig. 14 shows the measured A-phase PCC voltage and grid current without using the active damping control. It can be seen that the system becomes unstable in the cases with LCL resonance frequencies below $\omega_s/6$. This agrees well with the frequency-domain analysis in Fig. 8.

Figs. 15 and 16 compare the conventional capacitor-current-based active damping and the proposed virtual series R-C damper. The step response of grid current is tested. The measured results with the conventional active

damping method is shown in Fig. 15. The current control keeps stable in the cases of L_g=0 mH and L_g=9 mH, but it is unstable for L_g=4.5 mH. Furthermore, the transient oscillation in Fig. 5 (c) indicates the less damping in the case of L_g=9 mH. Fig. 16 shows the measured results with the proposed scheme. The system keeps stable in all the cases. The transient performance of the step response is also improved with more damping. These tests confirm both the frequency-domain analysis in Figs. 9 and 10, and the *z*-domain root locus analysis in Fig. 11.

B. Harmonic Compensation

To evaluate the effect of the proposed active damping on harmonic resonant controllers, the square waveform is generated from the AC power source and the grid current is controlled to be sinusoidal. Two different designs of the high-pass filters with the parameters given in Fig. 13 are compared by the harmonic spectra of grid current.

Fig. 17 shows the measured PCC voltage and grid current with low cut-off frequency of the high-pass filter, $\omega_{rc}=0.2\omega_s$. Fig. 17 (a) show the test results in the case of L_g=0 mH, in which up to the 43rd harmonics can be controlled by the resonant controllers with the phase leading angle derived by (1). However, as the increase of L_g, the decrease of the *LCL* resonance frequency reduces the frequency region of the harmonic compensation. Only
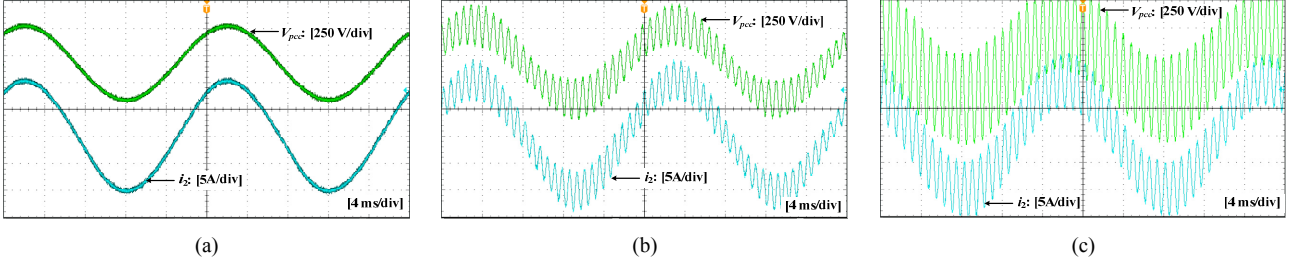
Fig. 14. Measured A-phase PCC voltage and grid current without using the active damping control. (a) L_g=0 mH. (b) L_g=4.5 mH. (c) L_g=9 mH.
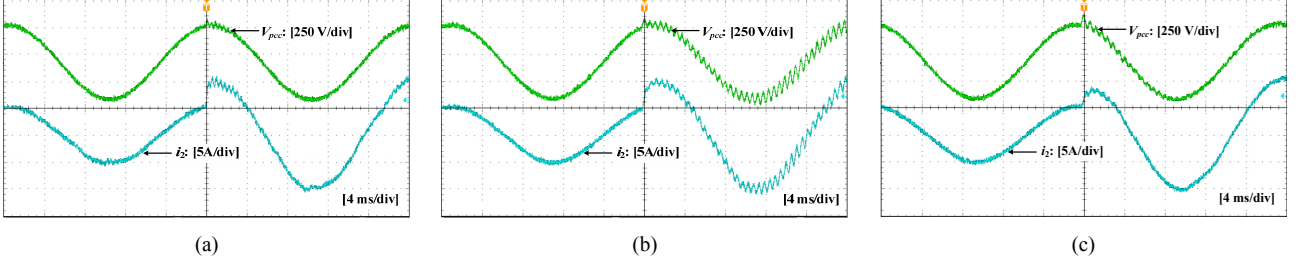

Fig. 15. Measured A-phase PCC voltage and grid current with the conventional active damping control. (a) L_g=0 mH. (b) L_g=4.5 mH. (c) L_g=9 mH.
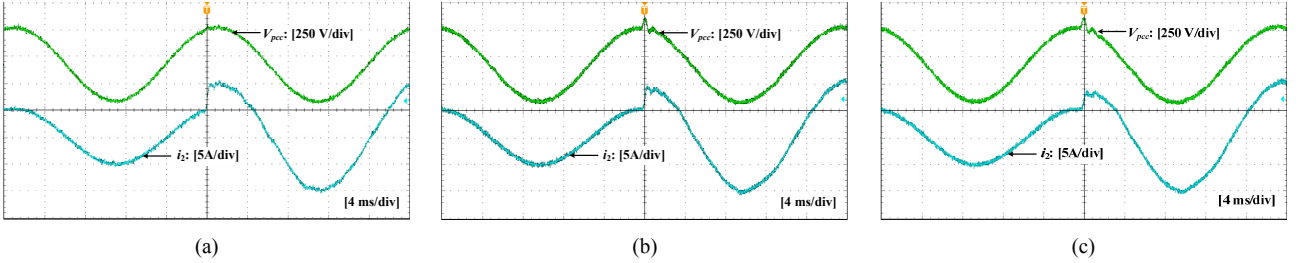

Fig. 16. Measured A-phase PCC voltage and grid current with the proposed active damping control. (a) L_g=0 mH. (b) L_g=4.5 mH. (c) L_g=9 mH.
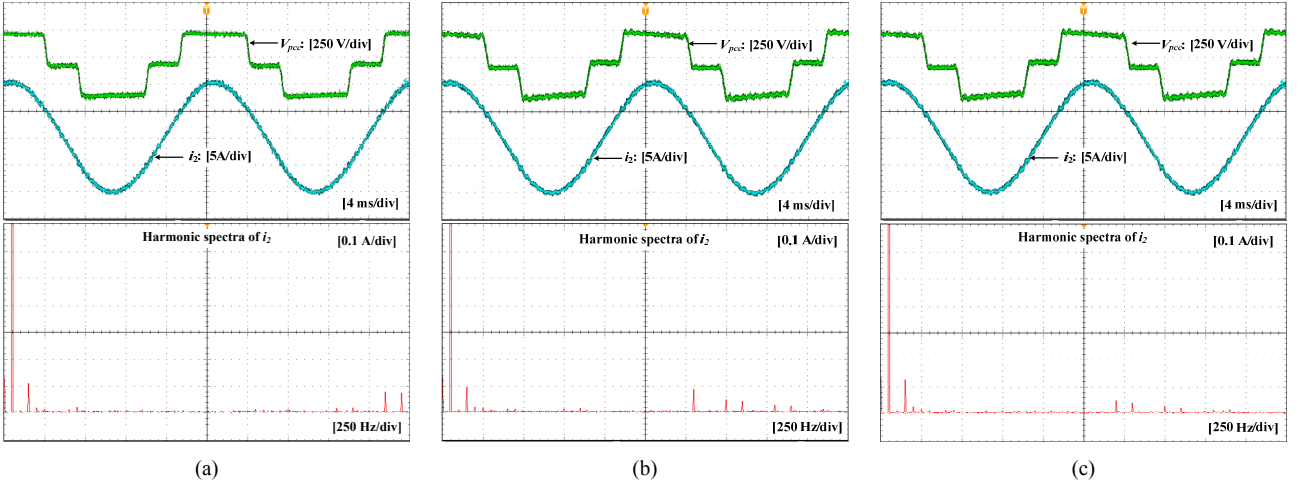

Fig. 17. Measured A-phase PCC voltage and grid current with the low cut-off frequency of high-pass filter (ω_{rc}=0.2ω_s) for harmonic compensation. (a) L_g=0 mH. (b) L_g=4.5 mH. (c) L_g=9 mH.

the harmonics up to 29th and 25th are controlled in Fig. 17 (b) and (c), respectively.

Fig. 18 shows the measured waveforms with the high cut-off frequency of the high-pass filter, ω_{rc}=3ω_s. The phase lag effect resulting from the increase of the cut-off frequency of high-pass filter can be clearly observed in Figs. 18 (b) and (c). Compared to Figs. 17 (b) and (c), it is seen that the 29th harmonics in Fig. 18 (b) and the 25th harmonics in Fig. 18 (c) are not compensated. The results in Fig. 17 (c) and Fig. 18 (c) confirm the analysis result

in Fig. 13. In contrast, the small discrepancy between Fig. 17 (a) and Fig. 18 (a) indicates that the increase of grid inductance exacerbates the phase lag effect caused by the high-pass filter.

VI. CONCLUSIONS

This paper has discussed the stability of the capacitor-current-based active damping and resonant controllers for current harmonics control. A virtual series R-C damper in parallel with the filter capacitor has been proposed, which
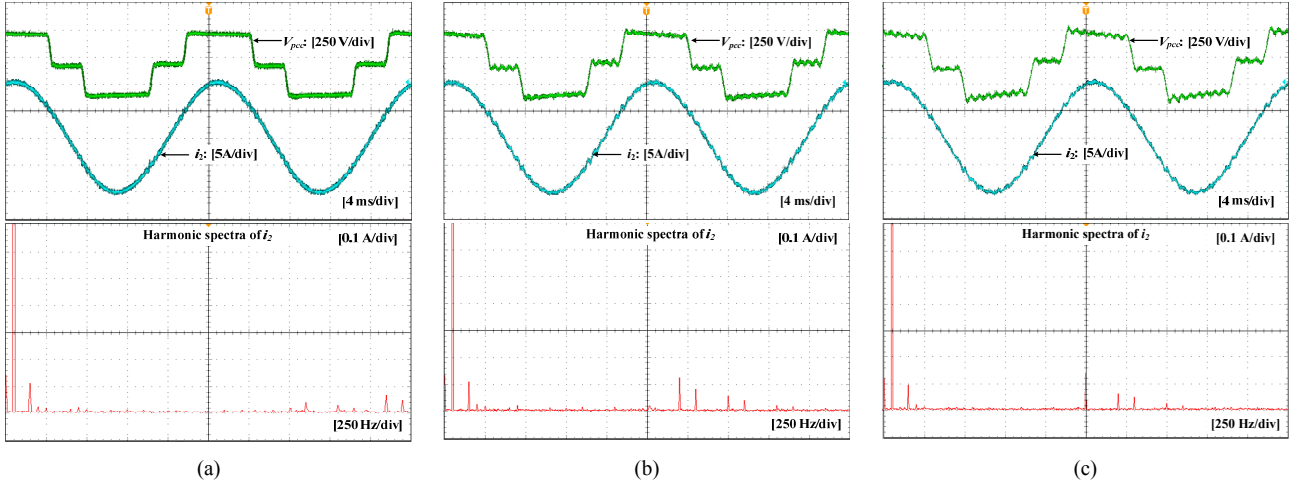
Fig. 18. Measured A-phase PCC voltage and grid current with the high cut-off frequency of high-pass filter ($\omega_{rc}=3\omega_s$) for harmonic compensation. (a) L_g=0 mH. (b) L_g=4.5 mH. (c) L_g=9 mH.

is realized by means of a first-order high-pass filter in the capacitor current feedback loop. The instability effect of computation and PWM delays in conventional capacitor current based active damping is addressed. A design-oriented analysis of the proposed active damping concept has been presented considering the interaction with the high-order harmonic resonant controllers under the wide variation of grid impedance. The design constraints of the high-pass filter have been analyzed by the z-domain root locus analysis and in the continuous frequency-domain. The experimental case studies validated the theoretical analysis and the performance of the proposed approach.

REFERENCES

[1] M. Liserre, F. Blaabjerg, and S. Hansen, "Design and control of an LCL-filter-based three-phase active rectifiers," *IEEE Trans. Ind. Appl.*, vol. 41, no. 5, pp. 1281-1291, Sept./Oct. 2005.
[2] E. Twining and D. G. Holmes, "Grid current regulation of a three-phase voltage source inverter with an LCL input filter," *IEEE Trans. Power Electron.*, vol. 18, no. 3, pp. 888-895, May 2003.
[3] X. Wang, F. Blaabjerg, and W. Wu, "Modeling and analysis of harmonic stability in an AC power-electronics-based power system," *IEEE Trans. Power Electron.*, in press, Feb. 2014.
[4] X. Wang. F. Blaabjerg, M. Liserre, Z. Chen, J. He, and Y. W. Li, "An active damper for stabilizing power-electronics-based AC systems," *IEEE Trans. Power Electron.*, vol. 29, no. 7, pp. 3318-3329, Jul. 2014.
[5] X. Wang, F. Blaabjerg, and Z. Chen, "Synthesis of variable harmonic impedance in inverter-interfaced distributed generation unit for harmonic damping throughout a distribution network," *IEEE Trans. Ind. Appl.*, vol. 48, no. 4, pp. 1407-1417, Jul./Aug. 2012.
[6] A. G. Yepes, F. Freijedo, J. Gandoy, O. Lopez, J. Malvar, and P. Comesana, "Effects of discretization methods on the performance of resonant controllers," *IEEE Trans. Power Electron.*, vol. 25, no. 7, pp. 1692-1712, Jul. 2010.
[7] A. G. Yepes, F. D. Freijedo, O. Lopez, and J. D. Gandoy, "Analysis and design of resonant current controllers for voltage-source converters by means of Nyquist diagrams and sensitive function," *IEEE Trans. Ind. Electron.*, vol. 58, no. 11, pp. 5231-5250, Nov. 2011.
[8] A. G. Yepes, F. Freijedo, O. Lopez, and J. Gandoy, "High-performance digital resonant controllers implemented with two integrators," *IEEE Trans. Power Electron.*, vol. 26, no. 2, pp. 563-576, Feb. 2011.
[9] F. Wang, J. L. Duarte, M. A. M. Hendrix, and P. F. Ribeiro, "Modeling and analysis of grid harmonic distortion impact of aggregated DG inverters," *IEEE Trans. Power Electron.*, vol. 26, no. 3, pp. 786-797, Mar. 2011.
[10] M. Liserre, R. Teodorescu, and F. Blaabjerg, "Stability of photovoltaic and wind turbine grid-connected inverters for a large set of grid impedance values," *IEEE Trans. Power Electron.*, vol. 21, no. 1, pp. 263-272, Jan. 2006.
[11] Z. Li, Y. Li, P. Wang, H. Zhu, C. Liu, and F. Gao, "Single-loop digital control of high-power 400-Hz ground power unit for airplanes," *IEEE Trans. Ind. Electron.*, vol. 57, no. 2, pp. 532-543, Feb. 2010.
[12] R. Venturini, P. Mattavelli, P. Zanchetta, M. Sumner, "Adaptive selective compensation for variable frequency active power filters in more electrical aircraft," *IEEE Trans. Aero. Electron. Syst.*, vol. 48, no. 2, pp. 1319-1328, Apr. 2012.
[13] R. N. Beres, X. Wang, F. Blaabjerg, C. L. Bak, and M. Liserre, "A review of passive filters for grid-connected voltage source converters," in *Proc. IEEE APEC* 2014, in press.
[14] J. Dannehl, M. Liserre, and F. W. Fuchs, "Filter-based active damping of voltage source converters with LCL filter," *IEEE Trans. Ind. Electron.*, vol. 58, no. 8, pp. 3623-3633, Aug. 2011.
[15] J. Dannehl, F. W. Fuchs, S. Hansen, and P. B. Thogersen, "Investigation of active damping approaches for PI-based current control of grid-connected pulse width modulation converters with LCL filters," *IEEE Trans. Ind. Appl.*, vol. 46, no. 4, pp. 1509-1517, Jul./Aug. 2010.
[16] S. Parker, B. P. McGrath, and D. G. Holmes, "Region of active damping control for LCL filters," *IEEE Trans. Ind. Appl.*, vol. 50, no. 1, pp. 424-432, Jan./Feb. 2014.
[17] Y. Lei, Z. Zhao, F. He, S. Lu, and L. Yin, "An improved virtual resistance damping method for grid-connected inverters with LCL filters," in *Proc. IEEE ECCE* 2011, pp. 3816-3822.
[18] C. Bao, X. Ruan, X. Wang, W. Li, D. Pan, and K. Weng, "Step-by-step controller design for LCL-type grid-connected inverter with capacitor-current-feedback active-damping," *IEEE Trans. Power Electron.*, vol. 29, no. 3, pp. 1239-1253, Mar. 2014.
[19] D. Pan, X. Ruan, C. Bao, W. Li, and X. Wang, "Capacitor-current-feedback active damping with reduced computation delay for improving robustness of LCL-type grid-connected inverter," *IEEE Trans. Power Electron.*, vol. 29, no. 7, pp. 3414-3427, Jul. 2014.
[20] V. Miskovic, V. Blasko, T. Jahns, A. Smith, C. Romenesko, "Observer based active damping of LCL resonance in grid connected voltage source converters" in *Proc. IEEE ECCE* 2013, pp. 4850-4856.
[21] M. Wagner, T. Barth, C. Ditmanson, R. Alvarez, and S. Bernet, "Discrete-time optimal active damping of LCL resonance in grid connected converters by proportional capacitor current feedback," in *Proc. IEEE ECCE* 2013, pp. 721-727.
[22] L. Harnefors, M. Bongiorno, and S. Lundberg, "Input-admittance calculation and shaping for controlled voltage-source converters," *IEEE Trans. Ind. Electron.*, vol. 54, no. 6, pp. 3323-3334, Dec. 2007.
[23] S. Buso and P. Mattavelli, *Digital Control in Power Electronics*, San Francisco, CA: Morgan & Claypool Publ., 2006.